Source-Resolved Volatility and Oxidation State Decoupling in Wintertime Organic Aerosols in Seoul

Hwajin Kim[1,2,*], Jiwoo Jeong[1], Jihye Moon[1], Hyun Gu Kang[2,3]

[1]Department of Environmental Health Sciences, Graduate School of Public Health, Seoul National University, 08826 Seoul, South Korea
[2]Institute of Health and Environment, Graduate School of Public Health, Seoul National University, 08826 Seoul, South Korea
[3]Now at Multiphase Chemistry Department, Max Planck Institute for Chemistry, 55128 Mainz, Germany

Correspondence to: Hwajin Kim (khj0116@snu.ac.kr)

Abstract.

Organic aerosols (OA) are key components of wintertime urban haze, but the relationship between their oxidation state and volatility—critical for understanding aerosol evolution and improving model predictions—remains poorly constrained. While oxidation–volatility decoupling has been observed in laboratory studies, field-based evidence under real-world conditions is scarce, particularly during severe haze episodes. This study presents a field-based investigation of OA sources and their volatility characteristics in Seoul during a winter haze period, using a thermodenuder coupled with a high-resolution time-of-flight aerosol mass spectrometer (HR-ToF-AMS).

Positive matrix factorization resolved six OA factors: hydrocarbon-like OA, cooking, biomass burning, nitrogen-containing OA (NOA), less-oxidized oxygenated OA (LO-OOA), and more-oxidized OOA (MO-OOA). Despite having the highest oxygen-to-carbon ratio (~1.15), MO-OOA exhibited unexpectedly high volatility, indicating a decoupling between oxidation state and volatility. We attribute this to fragmentation-driven aging and autoxidation under stagnant conditions with limited OH exposure. In contrast, LO-OOA showed lower volatility and more typical oxidative behavior.

Additionally, NOA—a rarely resolved factor in wintertime field studies—was prominent during cold, humid, and stagnant conditions and exhibited chemical and volatility features similar to biomass burning OA, suggesting a shared combustion origin and meteorological sensitivity.

These findings provide one of the few field-based demonstrations of oxidation–volatility decoupling in ambient OA and highlight how source-specific properties and meteorology influence OA evolution. The results underscore the need to refine OA representation in chemical transport models, especially under haze conditions.

Keywords: Organic aerosol volatility, HR-ToF-AMS, Thermodenuder, elemental ratios, aging, fragmentation

1 Introduction

Atmospheric aerosols affect both human health and the environment by reducing visibility (Ghim et al., 2005; Zhao et al., 2013) and contributing to cardiovascular and respiratory diseases (Hamanaka et al., 2018; Manisalidis et al., 2020). In addition, aerosols play a significant role in climate change by scattering or absorbing solar radiation and modifying cloud properties (IPCC AR6). Among the various aerosol components—including sulfate, nitrate, ammonium, chloride, crustal materials, and water—organic aerosols (OA) are particularly important to characterize, as they account for 20–90% of submicron particulate matter (Zhang et al., 2007). Identifying OA sources and understanding their behavior are critical for effective air quality management; however, this is particularly challenging due to the vast diversity and dynamic nature of OA compounds, which originate from both natural and anthropogenic sources. Unlike inorganic aerosols, organic aerosols (OAs) evolve continuously through complex atmospheric reactions, influenced by emission sources, meteorological conditions, and aerosol properties (Jimenez et al., 2009; Hallquist et al., 2009; Robinson et al., 2007; Donahue et al., 2006; Ng et al., 2010; Cappa and Jimenez, 2010).

Volatility is a key parameter for characterizing organic aerosol (OA) properties, as it governs gas-to-particle partitioning behavior and directly influences particle formation yields (Sinha et al., 2023). The classification of OA species based on their volatility—from extremely low-volatility (ELVOC) to semi-volatile (SVOC) and intermediate-volatility (IVOC) compounds—is central to the conceptual framework of secondary OA (SOA) formation and growth (Donahue et al., 2006). It also affects atmospheric lifetimes and human exposure by determining how long aerosols remain suspended in the atmosphere (Glasius and Goldstein, 2016). Therefore, accurately capturing OA volatility is essential for improving predictions of OA concentrations and their environmental and health impacts. However, chemical transport models often significantly underestimate OA mass compared to observations (Matsui et al., 2009; Jiang et al., 2012; Li et al., 2017), largely due to incomplete precursor inventories and simplified treatment of processes affecting OA volatility. For instance, aging—through oxidation reactions such as functionalization and fragmentation—can significantly alter volatility by changing OA chemical structure (Robinson et al., 2007; Zhao et al., 2016). Early volatility studies primarily utilized thermal denuders (TD) coupled with various detection instruments to investigate the thermal properties of bulk OA (Huffman et al., 2008). The subsequent coupling of TD with the Aerosol Mass Spectrometer allowed for component-resolved volatility measurements, providing critical, quantitative insight into the properties of OA factors (e.g., SV-OOA vs. LV-OOA) across different regions (Paciga et al., 2016; Cappa and Jimenez, 2010). These component-resolved volatility data are often used to constrain the Volatility Basis Set (VBS)—the current state-of-

the-art framework for modeling OA partitioning and evolution (Donahue et al., 2006). However, a limitation in many field studies is that the TD-AMS thermogram data are rarely translated into quantitative VBS distributions for individual OA factors, which limits their direct use in chemical transport models. Furthermore, the volatility of OOA during extreme haze conditions, where the expected inverse correlation between oxidation (O:C) and volatility can break down (Jimenez et al., 2009), remains poorly characterized, particularly in East Asia's highly polluted winter environments. A recent study in Korea further highlighted the importance of accounting for such processes when interpreting OA volatility under ambient conditions (Kang et al., 2022). Given its central role in OA formation, reaction, and atmospheric persistence, volatility analysis is critical for bridging the gap between measurements and model performance.

Traditionally, due to the complexity and variability of OA, the oxygen-to-carbon (O:C) ratio has been used as a proxy for estimating volatility. In general, higher O:C values indicate greater oxidation and lower volatility (Jimenez et al., 2009). Accordingly, many field studies classify oxygenated OA (OOA) into semi-volatile OOA (SV-OOA) and low-volatility OOA (LV-OOA) based on their O:C ratios (Ng et al., 2010; Huang et al., 2010; Mohr et al., 2012). However, this relationship is not always straightforward. Fragmentation during oxidation can increase both O:C and volatility simultaneously, disrupting the expected inverse correlation (Jimenez et al., 2009). In laboratory experiments, yields of highly oxidized SOA have been observed to decrease due to fragmentation (Xu et al., 2014; Grieshop et al., 2009). These findings suggest that while O:C can offer useful insights, it is insufficient alone to represent OA volatility. Direct volatility measurements, especially when paired with chemical composition data, are necessary to improve our understanding of OA sources and aging processes.

In this study, we investigate the sources and volatility characteristics of OA in Seoul during winter. Wintertime OA presents additional challenges due to its high complexity. During winter, emissions from combustion sources such as biomass burning and residential heating significantly increase, contributing large amounts of primary OA (Kim et al., 2017). Meanwhile, low ambient temperatures and reduced photochemical activity affect the formation and evolution of secondary OA (SOA). Frequent haze events further complicate the aerosol properties by extending aging times and increasing particle loadings. These overlapping sources and atmospheric conditions make winter OA particularly difficult to characterize and predict. Despite Seoul's significance for air quality management, comprehensive studies on OA volatility during winter remain limited. To address these goals, we conducted real-time, high-resolution measurements using a high-resolution time-of-flight aerosol mass spectrometer (HR-ToF-AMS) coupled with a thermodenuder (TD). The objectives of this study are to: (1) improve the understanding of

89 wintertime OA in Seoul, (2) characterize the volatility of OA associated with different sources, and (3) explore the
90 relationship between OA volatility and chemical composition.

2 Experimental methods

2.1 Sampling Site and Measurement Period

93 We conducted continuous real-time measurements in Seoul, South Korea, from 28 November to 28 December 2019.
94 The sampling site was located in the northeastern part of the city (37.60° N, 127.05° E), approximately 7 km from
95 the city center, surrounded by major roadways and mixed commercial–residential land use. Air samples were
96 collected at an elevation of approximately 60 meters above sea level, on the fifth floor of a building. A detailed site
97 description has been reported previously for winter Seoul (Kim et al., 2017). During this period, the average
98 ambient temperature was 1.76 ± 4.3 °C, and the average relative humidity (RH) was $56.9 \pm 17.5\%$, based on data
99 from the Korea Meteorological Administration (http://www.kma.go.kr).

2.2 Instrumentation and Measurements

101 The physico-chemical properties of non-refractory PM_1 (NR-PM_1) species—including sulfate, nitrate, ammonium,
102 chloride, and organics—were measured using an Aerodyne high-resolution time-of-flight aerosol mass
103 spectrometer (HR-ToF-AMS) (DeCarlo et al., 2006). PM_1 mass in this study is taken as NR-PM_1 (from AMS) +
104 black carbon (BC; measured by MAAP), which is appropriate for winter Seoul where refractory PM_1 (metal/sea-
105 salt/crustal) is minor and dust events were excluded (e.g., Kim et al., 2017; Nault et al., 2018; Kang et al., 2022;
106 Jeon et al., 2023).Data were acquired at 2.5-minute intervals, alternating between V and W modes. The V mode
107 provides higher sensitivity but lower resolution, suitable for mass quantification, whereas the W mode offers higher
108 mass resolution but lower sensitivity, used here for OA source apportionment. Simultaneously, black carbon (BC)
109 concentrations were measured at 1-minute intervals using a multi-angle absorption photometer (MAAP; Thermo
110 Fisher Scientific, Waltham, MA, USA). Total PM_1 mass was calculated as the sum of NR-PM_1 and BC.

111 Hourly trace gas concentrations (CO, O_3, NO_2, SO_2) were obtained from the Gireum air quality monitoring station
112 (37.61° N, 127.03° E), managed by the Seoul Research Institute of Public Health and Environment. Meteorological

113   data (temperature, RH, wind speed/direction) were collected from the nearby Jungreung site (37.61° N, 127.00° E).

114   All data are reported in Korea Standard Time (UTC+9).

115   To examine aerosol volatility, a thermodenuder (TD; Envalytix LLC) was installed upstream of the HR-ToF-AMS.

116   Details are provided in Supplementary Section S1 Kang et al. (2022). Briefly, ambient flow alternated every 5

117   minutes between a TD line and a bypass line at 1.1 L min⁻¹. Residence time in the TD line was ~6.3 s. The TD

118   setup included a 50 cm heating section followed by an adsorption unit. Heated particles were stripped of volatile

119   species, while the downstream carbon-packed section prevented recondensation. TD temperature cycled through

120   12 steps (30 to 200 °C), with each step lasting 10 min (total cycle = 120 min). AMS V and W modes were alternated

121   during the same cycle. The heater was pre-adjusted to the next temperature while the bypass was active.

122

123   **2.3 Data Analysis**

124

125   **2.3.1 Data analysis and OA Source Apportionment**

126   HR-AMS data were processed using SQUIRREL v1.65B and PIKA v1.25B. Mass concentrations of non-refractory

127   PM$_1$ (NR-PM$_1$) species were derived from V-mode data, while high-resolution mass spectra (HRMS) and the

128   elemental composition of organic aerosols (OA) were obtained from W-mode data. NR-PM$_1$ quantification

129   followed established AMS protocols (Ulbrich et al., 2009; Zhang et al., 2011). Both the bypass and TD streams

130   were processed using a time-resolved, composition-dependent collection efficiency CE(t) following Middlebrook

131   et al. (2012). TD heating can modify particle water and phase state/mixing and thereby influence CE beyond

132   composition (Huffman et al., 2009), but prior TD–AMS studies indicate that such effects are modest and largely

133   multiplicative, which do not distort thermogram shapes or T$_{50}$ ordering (Faulhaber et al., 2009; Cappa & Jimenez,

134   2010). In our data, the CE(t) statistics for the two lines were similar (campaign-average CE: TD = 0.55 ± 0.08;

135   bypass = 0.53 ± 0.04; Δ = 0.02 ≈ 3.7%, below the combined uncertainty ≈ 0.09). We therefore report volatility

136   metrics with these line-specific CE(t) corrections applied and interpret potential residual CE effects as minor. For

137   organics,elemental ratios (O:C, H:C, and OM/OC) were calculated using the Improved-Ambient (IA) method

138   (Canagaratna et al., 2015). Positive Matrix Factorization (PMF) was applied to the HRMS of organics using the

139   PMF2 algorithm (v4.2, robust mode) (Paatero and Tapper, 1994). The HRMS and corresponding error matrices

140   from PIKA were analyzed using the PMF Evaluation Tool v2.05 (Ulbrich et al., 2009). Data pretreatment followed

141   established protocols (Ulbrich et al., 2009; Zhang et al., 2011). A six-factor solution (fPeak = 0; Q/Q_expected =

142   3.56) was selected as optimal (Fig. S1). The resolved OA sources included hydrocarbon-like OA (HOA; 14%; O:C

143 = 0.13), cooking-related OA (COA; 21%; O:C = 0.18), nitrogen-enriched OA (NOA; 2%; O:C = 0.22), biomass-

144 burning OA (BBOA; 13%; O:C = 0.25), less-oxidized oxygenated OA (LO-OOA; 30%; O:C = 0.68), and more-

145 oxidized oxygenated OA (MO-OOA; 20%; O:C = 1.15) (Figs. S2 and S3). Alternative five- and seven-factor

146 solutions were also evaluated. In the five-factor solution, the biomass burning source was not clearly resolved and

147 appeared to be distributed across multiple factors. In the seven-factor solution, BBOA was further split into two

148 separate factors without clear distinction or added interpretive value, making the six-factor solution the most

149 physically meaningful and interpretable (Figs. S4 and S5). To ensure the statistical robustness of this solution, we

150 calculated uncertainties for each PMF factor using the bootstrap method (100 iterations) with the PET toolkit (v2.05)

151 (EPA, 2014; Xu et al., 2018; Srivastava et al., 2021) (Table S2 and Fig. S13).

152

153 **2.3.2 Thermogram and Volatility Estimation**

154 The chemical composition dependent mass fraction remaining (MFR) was derived at each TD temperature by

155 dividing the corrected mass concentration of the TD line [p] by the average of the adjacent bypass lines [p-1] and

156 [p+1]. Thermograms were corrected for particle loss, estimated using reference substances like NaCl, which exhibit

157 minimal evaporation (Huffman et al., 2009; Saha et al., 2014; Kang et al., 2022). OA factor concentrations at each

158 TD temperature were derived via multivariate linear regression between post-TD HRMS and ambient OA factor

159 HRMS profiles as described in Zhou et al., 2017.

160 Volatility distributions were modeled using the thermodenuder mass transfer model from Riipinen et al. (2010) and

161 Karnezi et al. (2014), implemented in Igor Pro 9 (Kang et al., 2022). OA mass was distributed into eight logarithmic

162 saturation concentration bins (C*: 1000 to 0.0001 $\mu g\,m^{-3}$). Modeled MFRs were fit to observations using Igor's

163 "FuncFit" function, repeated 1,000 times per OA factor to determine best-fit results. The model assumes no thermal

164 decomposition and includes adjustable parameters: mass accommodation coefficient (α_m) and enthalpy of

165 vaporization (ΔH_{exp}), randomly sampled within literature-based ranges (Table S1).

166

167 **3 Results and discussion**

168 **3.1 Overview of PM$_1$ Composition and OA Sources**

169 We conducted continuous measurements from 28 November to 28 December 2019, characterizing a winter period

170 with a mean PM$_1$ concentration of 27.8±15.3$\mu g\,m^{-3}$. This concentration is characterized as moderate; it closely

171 matches historical winter PM$_1$ means in Seoul (Kim et al., 2017) and implies an equivalent PM$_{2.5}$ concentration is

172 about 34.8μgm^{-3} (using a Korea-specific PM$_1$/PM$_{2.5}$≈0.8 (Kwon et al., 2023), which is near the national 24-h PM$_{2.5}$

173 standard (35μgm^{-3}) (AirKorea). The full co-evolution of PM$_1$, gaseous pollutants, and meteorological conditions

174 is provided in Fig. S6, showing an average ambient temperature of 1.76±4.3°C and average relative humidity (RH)

175 of 56.9±17.5% during the study.

176 Figure 1 summarizes the overall non-refractory submicron aerosol (NR-PM$_1$) composition and the identified OA

177 factors. Organics (41%) and nitrate (30%) were the most abundant chemical components of PM$_1$, followed by

178 ammonium (12%), sulfate (10%), BC (5%), and chloride (3%) (Fig. 1a). Among the organic aerosols, six OA

179 factors were identified during the winter of 2019: hydrocarbon-like OA (HOA; 14%; O:C = 0.13), cooking-related

180 OA (COA; 21%; O:C = 0.18), nitrogen-enriched OA (NOA; 2%; O:C = 0.22), biomass burning OA (BBOA; 13%;

181 O:C = 0.25), and two types of secondary organic aerosols—less-oxidized oxygenated OA (LO-OOA; 30%; O:C =

182 0.68) and more-oxidized oxygenated OA (MO-OOA; 20%; O:C = 1.15) (Fig. 1e and Fig. S2). These compositions

183 are consistent with previous wintertime observations in Kim et al. (2017), with the exception of newly resolved

184 NOA source. In the following sections, we describe each OA factor in the order of secondary OA (SOA), primary

185 OA (POA) and finally introduce NOA, which—while related to combustion POA—emerged as a distinct, nitrogen-

186 rich factor under the winter conditions of this study.

187 PM$_1$ mass concentrations varied widely, ranging from 4.61 to 91.4 μg m^{-3}, largely due to two severe haze episodes

188 that occurred between December 7–12 and December 22–26 (Fig. 1). During these episodes, average

189 concentrations increased significantly, driven primarily by elevated levels of nitrate and organic aerosols—

190 particularly MO-OOA and NOA (Fig. 1f,g). Back-trajectory clustering shows frequent short-range recirculation

191 over the Seoul Metropolitan Area during haze (Cluster 1; Fig. S8), and the time series indicates persistently low

192 surface wind speeds during these periods (1.73 ± 0.89 vs. 2.34 ± 1.18 (clean)) (Fig. S6). These patterns indicate

193 stagnation-driven accumulation of local emissions, consistent with the simultaneous increase of MO-OOA and

194 NOA that are examined in detail in subsequent sections. Such haze episodes, characterized by local emission

195 buildup and secondary aerosol production, are a typical wintertime feature, as also reported in Kim et al. (2017).

196 **3.1.1 Secondary organic aerosols (SOA)**

197 In this study, two OOA factors—more-oxidized OOA (MO-OOA) and less-oxidized OOA (LO-OOA)—were

198 identified, together accounting for approximately half of the total organic aerosol (OA) mass. This fraction is

199 notably higher than that reported in previous wintertime urban studies (Kim et al., 2017; Zhang et al., 2007). Both

OOAs exhibited characteristic mass spectral features, including prominent peaks at m/z 44 (CO_2^+) and m/z 43 ($C_2H_3O^+$), which are widely recognized as markers of oxygenated organics (Fig. S2e, S3f). The oxygen-to-carbon (O:C) ratios for MO-OOA and LO-OOA were 1.15 and 0.68, respectively, indicating both factors are highly oxidized relative to the primary OA factors (HOA, COA, BBOA) and that MO-OOA is substantially more oxidized than LO-OOA. The O:C ratio of MO-OOA was especially elevated, exceeding those reported in previous Seoul campaigns—0.68 in winter 2015 (Kim et al., 2017), 0.99 in spring 2019 (Kim et al., 2020), and 0.78 in fall 2019 (Jeon et al., 2023)—while the LO-OOA ratio was within a similar range.

MO-OOA showed strong correlations with secondary inorganic species such as nitrate ($r = 0.90$), ammonium ($r = 0.92$), and sulfate ($r = 0.81$), consistent with its formation through regional and local photochemical aging processes (Fig. S3). In contrast, LO-OOA exhibited only modest correlations with sulfate, nitrate, and ammonium ($r = 0.50$, 0.51, and 0.42, respectively). This weaker coupling indicates that LO-OOA represents a less aged oxygenated OA component (fresh SOA), distinguishable from the more aged, highly processed MO-OOA which tracks closely with secondary inorganic species. Regarding potential primary influence, LO-OOA does not exhibit a pronounced m/z 60 (levoglucosan) signal (Figs. S2 and 9). While the levoglucosan marker (f_{60}) is known to diminish with atmospheric aging and can become weak or undetectable downwind (Hennigan et al., 2010; Cubison et al., 2011), the absence of a distinct peak combined with the separation from inorganic salts suggests that LO-OOA is best characterized as freshly formed secondary organic aerosol likely originating from the rapid oxidation of local anthropogenic precursors.

3.1.2 Primary organic aerosols (POA)

Three primary organic aerosol (POA) factors were identified in this study: hydrocarbon-like OA (HOA), cooking-related OA (COA), and biomass burning OA (BBOA). These three components exhibited mass spectral and temporal characteristics consistent with previous observations in Seoul and other urban environments. HOA was characterized by dominant alkyl fragment ions ($C_nH_{2n+1}^+$ and $C_nH_{2n-1}^+$; Fig. S2a) and a low O:C ratio (0.13), consistent with traffic-related emissions (0.05–0.25) (Canagaratna et al., 2015). It showed strong correlations with vehicle-related ions $C_3H_7^+$ ($r = 0.79$) and $C_4H_9^+$ ($r = 0.86$) (Kim et al., 2017; Canagaratna et al., 2004; Zhang et al.,

225   2005), and exhibited a distinct morning rush hour peak (06:00–08:00), followed by a decrease likely driven by
226   boundary layer expansion (Fig. S3a).

227   COA, accounting for 21% of OA, showed higher contributions from oxygenated ions than HOA, with tracer peaks
228   at m/z 55,84 and 98 (Fig. S2b) consistent with cooking emissions (Sun et al., 2011). COA showed an enhanced
229   signal at m/z 55 relative to m/z 57, with a 55/57 ratio of 3.11, substantially larger than that of HOA (1.10). This
230   elevated ratio is consistent with previously reported AMS COA spectra in urban environments (e.g., Allan et al.,
231   2010; Mohr et al., 2012; Sun et al., 2011), supporting our factor assignment. It correlated strongly with cooking-
232   related ions such as $C_3H_3O^+$ (r = 0.94), $C_5H_8O^+$ (r = 0.96), and $C_6H_{10}O^+$ (r = 0.98) (Fig. S3h), and displayed
233   prominent peaks during lunch and dinner hours, reflecting typical cooking activity patterns.

234   BBOA was identified based on characteristic ions at m/z 60 ($C_2H_4O_2^+$) and 73 ($C_3H_5O^+$), both of which are
235   associated with levoglucosan—a well-established tracer for biomass burning (Simoneit et al., 2002). Its relatively
236   high f_{60} and low f_{44} values (Fig. S9) indicate that the BBOA observed in this study was relatively fresh and had not
237   undergone extensive atmospheric aging (Cubison et al., 2011). Regarding source location, several pathways can
238   influence Seoul's biomass burning signature. First, urban/peri-urban small-scale burning (e.g., solid-fuel use in
239   select households, restaurant charcoal use, and intermittent waste burning) has been reported and can enhance
240   BBOA locally (Kim et al., 2017). Second, nearby agricultural-residue burning in surrounding provinces occurs
241   seasonally and can episodically impact the metropolitan area (Han et al., 2022). Third, regional transport from
242   upwind regions (e.g., northeastern China/North Korea) can bring biomass burning influenced air masses under
243   northerly/northwesterly flow (Lamb et al., 2018; Nault et al., 2018). In this dataset, the nighttime and early-
244   morning enhancements and trajectory clusters showing regional recirculation indicate a predominantly local/near-
245   source contribution during the study period, with episodic non-local influences remaining possible (Fig. S8).

246   **3.1.~~3~~2.1 Nitrogen-containing organic aerosol (NOA)**

247   A distinct nitrogen-containing organic aerosol (NOA) factor was resolved in this study, whereas earlier wintertime
248   AMS–PMF analyses in Seoul did not isolate such a component. The NOA factor exhibited the highest nitrogen-to-
249   carbon (N:C) ratio (0.22) and the lowest oxygen-to-carbon (O:C) ratio (0.19) among all POA factors (Fig. S2),
250   indicating a chemically reduced, nitrogen-rich composition. The NOA mass spectrum was dominated by amine-
251   related fragments including m/z 30 (CH_4N^+), 44 ($C_2H_6N^+$), 58 ($C_3H_8N^+$), and 86 ($C_5H_{12}N^+$) (Fig. 3a). The spectral
252   signature of the factor is defined by the characteristic dominance of the m/z 44 fragment, which typically serves as

253   the primary marker for dimethylamine (DMA)-related species, closely followed by m/z 58 (trimethylamine, TMA)

254   and m/z 30 (methylamine, MA). This profile is in strong agreement with NOA factors resolved via PMF in other

255   polluted environments. For instance, the dominance of m/z 44 and m/z 30 aligns with amine factors reported in

256   New York City (Sun et al., 2011) and Pasadena, California (Hayes et al., 2013). This DMA-dominated signature is

257   also consistent with seasonal characterization of organic nitrogen in Beijing (Xu et al., 2017) and Po Valley, Italy

258   (Saarikoski et al., 2012), reinforcing the common chemical signature of reduced organic nitrogen across diverse

259   urban and regional environments.

260   In this study, NOA contributed approximately 2 % of total OA, comparable to urban contributions reported in

261   Guangzhou (3 %; Chen et al., 2021), Pasadena (5 %; Hayes et al., 2013), and New York (5.8 %; Sun et al., 2011).

262   These similarities suggest that the NOA factor observed in Seoul reflects a broader class of urban wintertime

263   reduced-nitrogen aerosols rather than a site-specific anomaly. Furthermore, the presence of non-negligible signals

264   at m/z 58 and m/z 86 supports the contribution of slightly larger alkylamines, a pattern that aligns well with

265   established AMS laboratory reference spectra (Ge et al., 2011; Silva et al., 2008). In most urban environments, the

266   detectability of NOA appears to depend strongly on the interplay between emission strength, stagnation, and

267   humidity—which together govern the particle-phase partitioning of volatile amines.

268   Furthermore, the presence of non-negligible signals at m/z 58 and m/z 86 supports the contribution of slightly larger

269   alkylamines, a pattern that aligns well with established AMS laboratory reference spectra for these reduced nitrogen

270   compounds (Ge et al., 2011; Silva et al., 2008).

271   These amines are commonly emitted during the combustion of nitrogen-rich biomass and proteinaceous materials

272   and are frequently associated with biomass-burning emissions (Ge et al., 2011). Previous molecular analyses in

273   Seoul also indicate DMA, MA, and TMA as the dominant amine species in December (Baek et al., 2022). While

274   other amines such as triethylamine (TEA), diethylamine (DEA), and ethylamine (EA) may contribute via

275   industrial/solvent pathways (e.g., chemical manufacturing, petrochemical corridors, wastewater treatment), our

276   HR-AMS spectra are dominated by small alkylamine fragments (m/z 30, 44, 58, 86) and the diurnal behavior co-

277   varies with combustion markers (Fig. 2), indicating a primarily combustion-linked influence. Nevertheless, recent

278   urban measurements and sector-based analyses show that industrial activities can contribute measurable amines in

279   cities (Tiszenkel et al., 2024; Zheng et al., 2015; Mao et al., 2018; Shen et al., 2017; Yao et al., 2016). Accordingly,

280   a minor NOA contribution from solvent/industrial amines cannot be excluded. NOA exhibited a nighttime–early-

morning enhancement (Fig. 2a), similar to BBOA, indicating that both factors are influenced by wintertime combustion and residential heating, which are known sources of small alkylamines and amides (You et al., 2014; Yao et al., 2016). Strong correlations of NOA with CH_4N^+ (r = 0.95) and $C_2H_6N^+$ (r = 0.91) (Fig. 2) further support the presence of reduced-nitrogen species associated with these combustion activities. However, the time series of NOA and BBOA are not strongly correlated (Fig. 2 and Fig. S7). This contrast reflects their differing behaviors: BBOA follows a relatively regular daily emission pattern, whereas NOA appears predominantly during stagnant haze periods (Fig. 1) when cold, humid, and low-wind conditions allow semi-volatile amines to partition to the particle phase and form low-volatility aminium salts. Thus, NOA in wintertime Seoul likely reflects a combination of shared primary combustion influences and enhanced secondary processing of amine-containing precursors under meteorological conditions that favor partitioning and accumulation.

Detection of particulate NOA using real time measurement has been challenging due to its low concentration and high volatility. Although Baek et al. (2022) identified nitrogen-containing species in Seoul via year-round filter-based molecular analysis, PMF-based resolution of NOA in real time has not been previously reported. The successful identification in this study is likely attributable to favorable winter meteorological conditions—specifically low temperatures (–0.24 °C) and persistently high relative humidity (~57%) compared to the 2017 winter season (Kim et al., 2017)—that enhanced gas-to-particle partitioning of semi-volatile amines, thereby enabling their detection (Fig. S2). NOA concentrations frequently exceeded 1 μg m^{-3} when RH surpassed 60% (Fig. 2), supporting the importance of RH-driven partitioning and the subsequent formation of low-volatility aminium salts (Rovelli et al., 2017). Although extremely low temperatures may inhibit NOA formation due to the transition of aerosol particles into solid phase (Ge et al., 2011; Srivastava et al., 2022), the combination of consistently cold and humid conditions during the measurement period likely promoted the partitioning of semi-volatile amines into the particle phase. In addition, episodic haze events further elevated NOA levels, increasing its contribution to OA from 1% during clean periods to as much as 3% (Fig. 1f–h). These high-concentration events likely improved the signal-to-noise ratio, facilitating PMF resolution. Back-trajectory clustering indicates that NOA-enhanced events were dominated by short-range recirculation (Cluster 1; Fig. S7), consistent with the short atmospheric lifetimes and high reactivity of alkylamines (Nielsen et al., 2012; Hanson et al., 2014). Overall, the factor reflects semi-volatile, reduced-nitrogen species originating from primary urban combustion sources, with their observed particle-phase mass amplified by rapid secondary partitioning and salt formation under seasonally favorable conditions.

3.2 Volatility of Non-Refractory Species

Figure 4 presents thermograms of non-refractory (NR) species measured by HR-ToF-AMS. The mass fraction remaining (MFR) after thermodenuder (TD) treatment follows the typical volatility trend reported in previous studies (Xu et al., 2016; Kang et al., 2022; Jeon et al., 2023; Huffman et al., 2009): nitrate was the most volatile, followed by chloride, ammonium, organics, and sulfate. Nitrate showed the steepest decline with increasing temperature, with a T_{50} of ~67 °C—substantially higher than that of pure ammonium nitrate (~37 °C; Huffman et al., 2009). At 200 °C, ~2% of the initial nitrate signal remained (Fig. 4). Since pure ammonium nitrate fully evaporates well below this temperature (Huffman et al., 2009), this small residual fraction likely represents the least volatile portion of organic nitrates. Compared to previously reported fall conditions (T_{50} ~73 °C, incomplete evaporation), winter nitrate appeared more volatile, indicating relatively fewer non-volatile nitrate forms (e.g., Kang et al., 2022; Jeon et al., 2023). Sulfate exhibited the highest thermal stability among the measured species. The thermogram showed a relatively stable mass fraction (MFR > 0.8) up to ~130 °C, followed by a sharp decline at temperatures above 140 °C (Fig. 4). This profile is consistent with the typical volatilization behavior of ammonium sulfate in TD-AMS, which requires higher temperatures to evaporate compared to nitrate or organics (Huffman et al., 2009). At 200 °C, approximately 25% of the sulfate mass remained. This residual suggests the presence of a sulfate fraction with lower volatility than pure ammonium sulfate, likely associated with organosulfates or low-volatility mixtures, whereas refractory metal sulfates are not efficiently detected by the AMS (Canagaratna et al., 2007). Ammonium showed intermediate volatility, with T_{50} between nitrate and sulfate. Its slightly lower winter T_{50} suggests stronger nitrate association. Residual ammonium at 200 °C was consistent (~4%) in previously reported spring/fall measurements (Kang et al., 2022; Jeon et al., 2023). Chloride volatility was broadly consistent with prior AMS studies, with T_{50} values comparable across seasons (e.g., Xu et al., 2016; Jeon et al., 2023). The near-complete evaporation observed in winter (~4% residual at 200 °C, Fig. 4) indicates that the chloride measured here was dominated by volatile inorganic chloride, specifically ammonium chloride (NH_4Cl),

which fully evaporates at relatively low temperatures (Huffman et al., 2009). By contrast, metal chlorides (e.g., NaCl, KCl) are refractory and far less volatile; they are also poorly detected by the AMS (Canagaratna et al., 2007). The lower residual in winter compared to fall (~10%) therefore suggests that wintertime chloride consisted almost exclusively of pure ammonium chloride, whereas the fall samples may have contained a minor fraction of less volatile or refractory chloride species. Organics exhibited moderate volatility (T_{50} ~120 °C), and their thermogram showed a gradual, continuous decrease in mass fraction with increasing TD temperature. This smooth profile reflects the presence of a broad distribution of organic compounds spanning SVOC to LVOC ranges, in contrast to inorganic species such as nitrate or ammonium chloride, which often show more abrupt losses at characteristic temperatures (Huffman et al., 2009; Xu et al., 2016). This behavior is consistent with previous TD-AMS observations in Seoul during spring and fall (Kang et al., 2022; Jeon et al., 2023).

3.2.1 Volatility Profiles of Organic sources

Figure 5 presents the volatility distributions of six OA sources within the volatility basis set (VBS) framework. Volatility is expressed as the effective saturation concentration (C^*, $\mu g\,m^{-3}$), where higher C^* values correspond to higher volatility. Following Donahue et al. (2009), C^* values are categorized into four bins: extremely low-volatility organic compounds (ELVOCs, $\log C^* < -4.5$), low-volatility organic compounds (LVOCs, $-4.5 < \log C^* < -0.5$), semi-volatile organic compounds (SVOCs, $-0.5 < \log C^* < 2.5$), and intermediate-volatility organic compounds (IVOCs, $2.5 < \log C^* < 6.5$).

Among the primary OA (POA) sources, hydrocarbon-like OA (HOA) exhibited the highest volatility, with mass predominantly distributed in the SVOC and IVOC ranges, consistent with its chemically reduced nature (O:C = 0.13) and direct combustion origin. Mass fraction remaining (MFR) results (Fig. S9) further support this, showing rapid mass loss at lower temperatures. Biomass burning OA (BBOA) and nitrogen-containing OA (NOA) also showed high volatility, peaking in the SVOC–IVOC range ($\log C^* = 1-3$), but displayed slightly higher O:C ratios (0.25 and 0.19, respectively). This modest enhancement in O:C reflects their source composition—biomass combustion produces partially oxygenated organic species (e.g., levoglucosan, phenols), and NOA contains nitrogen-bearing functional groups—rather than enhanced atmospheric oxidation. Cooking-related OA (COA) showed a more moderate volatility profile, with mass more evenly distributed across the LVOC and SVOC bins. This behavior differs from that of BBOA, which is slightly more oxidized yet more volatile. This apparent decoupling between oxidation state and volatility is a characteristic feature of COA reported in previous volatility studies (Paciga et al., 2016; Kang et al., 2022). These studies attribute the lower volatility of COA to its abundance

368 of high-molecular-weight fatty acids (e.g., oleic, palmitic, and stearic acids) and glycerides (Mohr et al., 2009; He

369 et al., 2010). Unlike the smaller, fragmented molecules typical of biomass burning, these lipid-like compounds

370 possess high molar masses that suppress volatility, even though their long alkyl chains result in low O:C ratios.

371 For secondary OA (SOA), less-oxidized oxygenated OA (LO-OOA) exhibited the lowest volatility, with substantial

372 mass in the LVOC and ELVOC bins ($C^* \approx 10^{-3}$–10^{-4}). This is in agreement with previous findings in Seoul during

373 spring (Kang et al., 2022). In contrast, more-oxidized OOA (MO-OOA), despite its higher oxidation state (O:C =

374 1.15), displayed greater volatility, with a peak at $C^* \approx 10^1$. This discrepancy likely reflects differences in formation

375 and aging processes, as discussed further in Section 3.3.

376 Overall, the volatility characteristics across OA factors suggest that oxidation state alone does not fully explain

377 volatility. Rather, volatility is shaped by a combination of emission source, emission timing, temperature, and

378 atmospheric processing. These findings highlight the importance of integrating both chemical and physical

379 characterization to better understand OA formation and aging across seasons.

380 **3.3 Aging effect on volatility from 2D VBS**

381 Generally, the oxygen-to-carbon (O:C) ratio of organic aerosols (OA) is inversely related to their volatility. As O:C

382 increases through aging, the effective saturation concentration (C^*) typically decreases, resulting in lower volatility

383 (Donahue et al., 2006; Jimenez et al., 2009). This relationship arises because oxidative functionalization introduces

384 polar groups (e.g., hydroxyl, carboxyl) that increase molecular weight and enhance intermolecular hydrogen

385 bonding, thereby reducing the effective saturation concentration (C^*) and promoting particle-phase retention

386 (Jimenez et al., 2009; Kroll and Seinfeld, 2008; Donahue et al., 2011). However, in this study, the most oxidized

387 OA factor—MO-OOA, with a high O:C ratio of 1.15—exhibited unexpectedly high volatility. Its volatility

388 distribution was skewed toward SVOCs and IVOCs (Fig. 5), and its rapid mass loss in MFR thermograms (Fig. S9)

389 further indicated low thermal stability. This observation appears to contradict the usual inverse O:C–volatility

390 relationship; however, under winter haze conditions—with suppressed O_3/low OH, particle-phase autoxidation and

391 fragmentation can yield higher-O:C yet more volatile products, with enhanced condensation on abundant particle

392 surface area (details below).

393 Viewed against prior TD-AMS results, the volatility of Seoul's winter MO-OOA presents a unique case,

394 particularly in the nature of its O:C-volatility relationship. Prior urban studies have commonly reported substantial

395 SVOC-OA, consistent with high photochemical activity or elevated loadings; for example, prior TD-AMS studies

14

in Mexico City, Los Angeles, Beijing, and Shenzhen have all reported substantial SVOC–IVOC contributions during polluted periods, indicating that high OA volatility is a common feature of urban environments across seasons (Cappa and Jimenez, 2010; Xu et al., 2019; Cao et al., 2018). While these comparisons establish that volatile OA is common, they generally did not report the factor-level inversion observed here, where the highly-oxidized OOA component (MO-OOA) was more volatile than a less-oxidized OOA (LO-OOA). This behavior is distinct from findings in colder, lower-loading regimes; wintertime Paris, for instance, maintained the conventional hierarchy where the more-oxidized OOA was comparatively less volatile (Paciga et al., 2016). Furthermore, seasonal context within Seoul showed springtime OA with lower oxidation levels than our winter MO-OOA despite similar SVOC contributions (Kang et al., 2022). This comprehensive comparison underscores the unusual nature of the O:C-volatility relationship observed under the specific winter haze conditions in Seoul.

3.3.1 High-volatility nature of MO-OOA in Seoul wintertime

MO-OOA exhibited high O:C ratios and high apparent volatility, characteristics that were further amplified during haze episodes—periods marked by reduced ozone levels, low solar radiation, and elevated aerosol mass concentrations (Fig. 7 and Fig. S6, yellow shading). Spectrally, MO-OOA was defined by a consistently high f_{44} (CO_2^+) signal and a comparatively stable f_{43} ($C_2H_3O^+$) signal relative to LO-OOA (Fig. 6). Notably, when MO-OOA concentrations intensified during haze, only f_{44} was significantly enhanced, while f_{43} remained nearly unchanged (Fig. 6). This trend is corroborated by the haze–non-haze comparison (Fig. S12), where haze periods (including high MO-OOA intervals) showed elevated contributions from oxygenated fragments (m/z 28, 29, 44) and higher O:C ratios. In contrast, non-haze periods were characterized by larger fractional contributions from hydrocarbon-like fragments (m/z 41, 43, 55, 57). The observed temporal pattern—elevated f_{44} without corresponding changes in f_{43}—is a typical signature of highly oxidized and fragmented organic aerosol (Figs. 6 and 7), suggesting that aging was dominated by fragmentation rather than functionalization (Kroll et al., 2009). These spectral patterns collectively indicate that MO-OOA is highly oxidized yet remains relatively volatile compared to LO-OOA.

The elevated volatility of MO-OOA despite its high O:C (~1.15) indicates that oxidation under these haze conditions did not follow the classical multi-generational OH-driven aging pathway, which typically increases molecular mass and reduces volatility. Instead, the data align with fragmentation-dominated aging, where highly oxygenated but lower-molecular-weight compounds (e.g., small acids or diacids) are formed. Prior field and

425 laboratory studies using online AMS/FIGAERO-CIMS and EESI-TOF have similarly reported high-O:C yet

426 volatile product distributions characterized by high f_{44} and stable f_{43} (Kroll et al., 2009; Ng et al., 2010; Chhabra et

427 al., 2011; Lambe et al., 2012; Lopez-Hilfiker et al., 2016; D'Ambro et al., 2017).

428 While direct mechanistic measurements were not available in this study, we hypothesize that the formation of this

429 volatile, high-O:C component may be driven by specific low-light oxidation pathways consistent with the observed

430 environmental conditions. The suppressed ozone levels during haze likely indicate a low-OH oxidation regime (Fig.

431 7). Under such conditions, radical chemistry involving NO_3 (which is longer-lived in low light) or particle-phase

432 autoxidation could preferentially produce highly oxygenated but relatively small organic fragments (Ehn et al.,

433 2014; Zhao et al., 2023). Although haze suppresses photolysis, HONO concentrations—maintained via

434 heterogeneous conversion or surface emissions—could still provide a non-negligible source of OH (Gil et al., 2021;

435 Kim et al., 2024; Slater et al., 2020). Furthermore, the high aerosol mass loadings during haze (C_{oa}) provide

436 abundant surface area for absorptive partitioning (Pankow, 1994; Donahue et al., 2006). This increased partitioning

437 mass allows even relatively volatile, oxidized compounds to condense into the particle phase, contributing to the

438 high apparent volatility and oxidation state observed (Jimenez et al., 2009; Ng et al., 2016). Consequently, these

439 results underscore the need for SOA models to incorporate fragmentation-dominated pathways to accurately

440 represent wintertime haze evolution.

441 **4 Conclusions**

442 This study provides a comprehensive characterization of wintertime submicron aerosols (PM_1) in Seoul, integrating

443 chemical composition, volatility measurements, and source apportionment to reveal critical insights into urban OA

444 evolution. The two most significant findings are the robust real-time identification of a nitrogen-containing organic

445 aerosol (NOA) factor and the observation of unexpected volatility behavior in highly oxidized OA. The NOA factor,

446 spectrally dominated by low-molecular-weight alkylamine fragments, was successfully resolved primarily due to

447 the accumulation of pollutants during wintertime stagnation, which sufficiently enhanced the spectral signals of

448 these semi-volatile species for identification. Its temporal and chemical characteristics point to a mixed

449 primary/secondary origin: driven by direct combustion emissions (e.g., residential heating) but significantly

450 enhanced by the rapid gas-to-particle partitioning of semi-volatile amines under cold, humid conditions.

451 Concurrently, the volatility analysis revealed ~~a striking~~a notable decoupling between oxidation state and volatility

452 for the More-Oxidized Oxygenated OA (MO-OOA). Despite its high O:C ratio (~1.15), MO-OOA exhibited

16

453 elevated volatility, a deviation from classical aging models that typically associate high oxidation with low
454 volatility. This behavior is attributed to the specific conditions of winter haze—reduced photolysis and high aerosol
455 mass loadings—which favor fragmentation-dominated aging pathways and the absorptive partitioning of volatile
456 oxygenated products.

457 These results revise our understanding of wintertime aerosol dynamics and underscore the limitations of current
458 models in representing reduced-nitrogen species and non-canonical oxidation pathways. To address the remaining
459 uncertainties, future research should prioritize evaluating the seasonal variability of NOA to better disentangle the
460 influence of meteorological drivers from specific emission sources. Concurrently, there is a critical need to directly
461 probe radical oxidation mechanisms, such as RO_2 autoxidation and NO_3 chemistry, particularly under haze
462 conditions. Integrating these field inquiries with laboratory studies and advanced molecular-level measurements
463 (e.g., FIGAERO-CIMS, EESI-TOF) will be essential for constraining the formation, lifetime, and climate impacts
464 of these complex organic aerosol components in polluted megacities.

Data availability.

Data presented in this article are available upon request to the corresponding author.

Acknowledgements

Author Contributions

Hwajin Kim designed and prepared the manuscript. Jiwoo Jeong operated the TD-AMS and analyse the data. Jihye Moon analyse the data. Hyungu Kang analyse the volatility of OA.

Competing interests.

The authors declare that they have no conflict of interest.

Tables and Figures
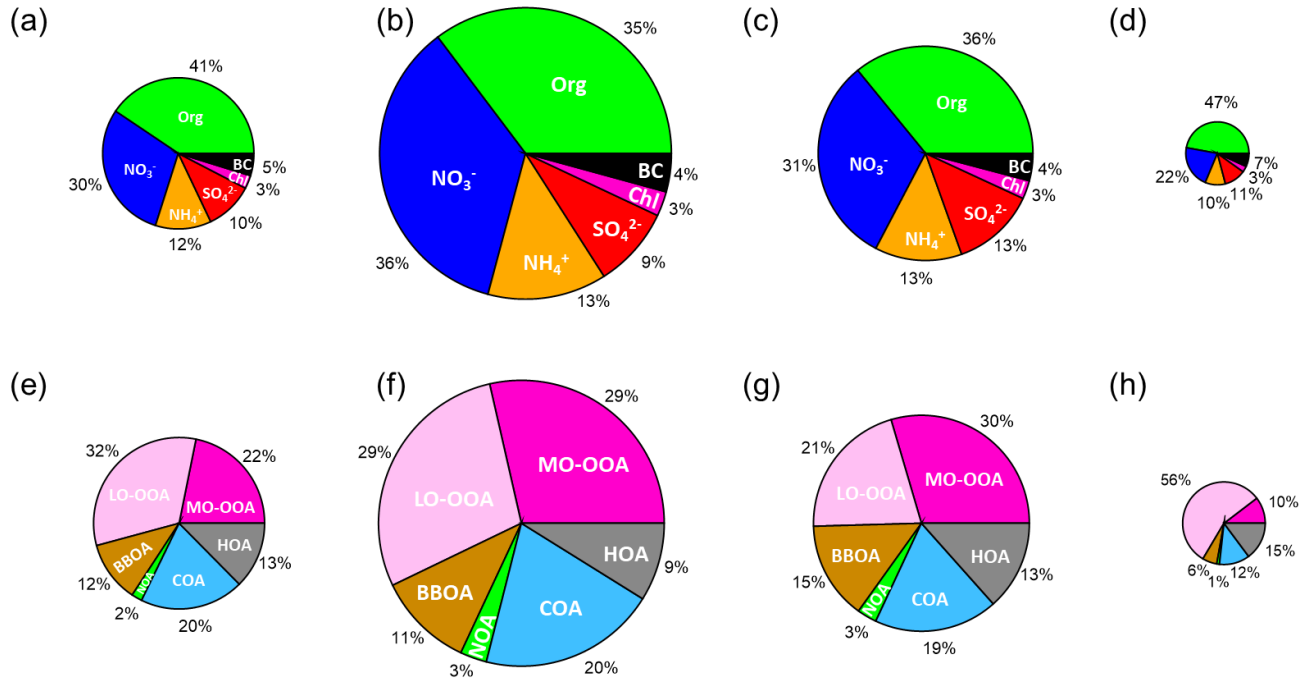
	Period	Standard	Avg. Mass conc.($\mu g\ m^{-3}$)
Total	2019.11.28 ~ 2019.12.28		Avg PM_1 = 26.37
Clean	2019.12.04 ~ 2019.12.06	Daily PM_1 < 10.00 $\mu g\ m^{-3}$	Avg PM_1 = 9.98
Haze 1	2019.12.07 ~ 2019.12.11	Daily PM_1 > 30.00 $\mu g\ m^{-3}$	Avg PM_1 = 51.88
Haze 2	2019.12.21 ~ 2019.12.25	Daily PM_1 > 30.00 $\mu g\ m^{-3}$	Avg PM_1 = 37.71

501
502 **Figure 1.** Compositional pie charts of PM_1 species for (a) the entire study period, (b) haze period 1, (c) haze period 2, and
503 (d) a clean period; and of each OA source for (e) the entire study period, (f) haze period 1, (g) haze period 2, and (h) the
504 clean period.Table. Standard and average PM_1 mass concentrations during the entire study period, haze period 1, haze period
505 2, and the clean period.

506
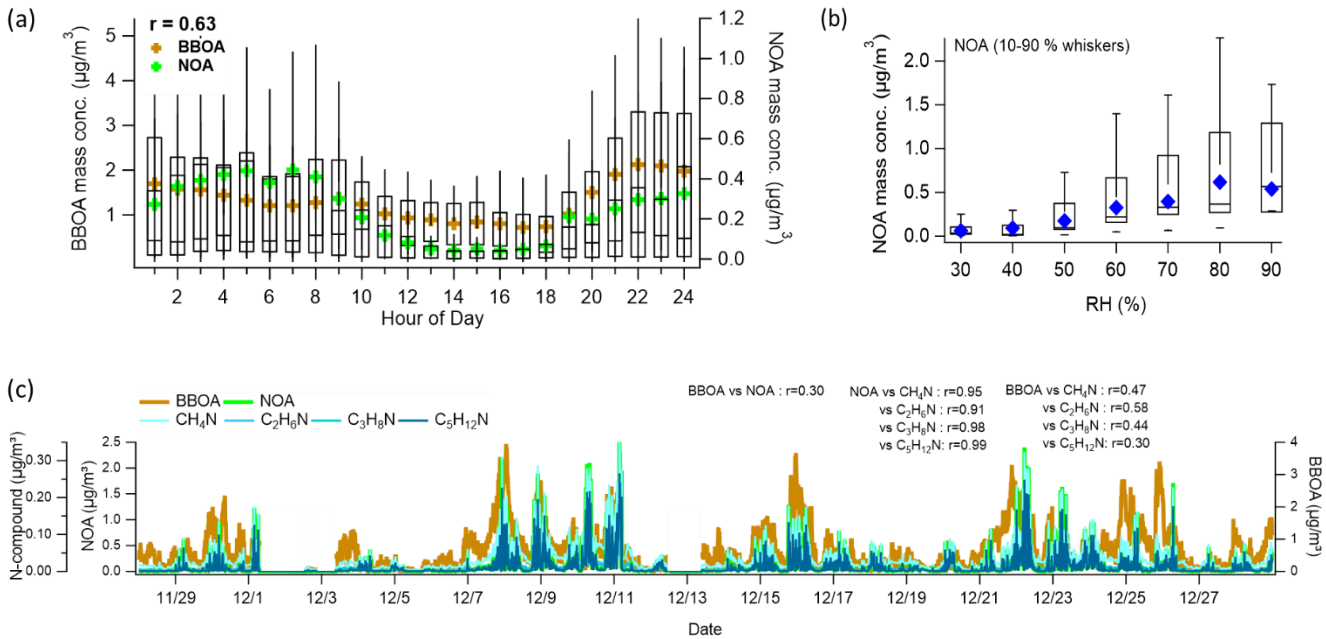
507

508 **Figure 2.** (a) Diurnal mean profiles of NOA and BBOA. Whiskers denote the 90th and 10th percentiles; box

509 edges represent the 75th and 25th percentiles; the horizontal line indicates the median, and the colored marker

510 shows the mean. The diurnal correlation between NOA and BBOA mean values is 0.63.

511 (b) Relative humidity (RH)-binned nighttime (19:00–05:00) profile of NOA. Box and whisker definitions are the

512 same as in panel (a). (c) Time series of NOA, BBOA, and amine-related ions (CH_4N^+, $C_2H_6N^+$, $C_3H_8N^+$,

513 $C_5H_{12}N^+$), along with their correlations with NOA and BBOA.
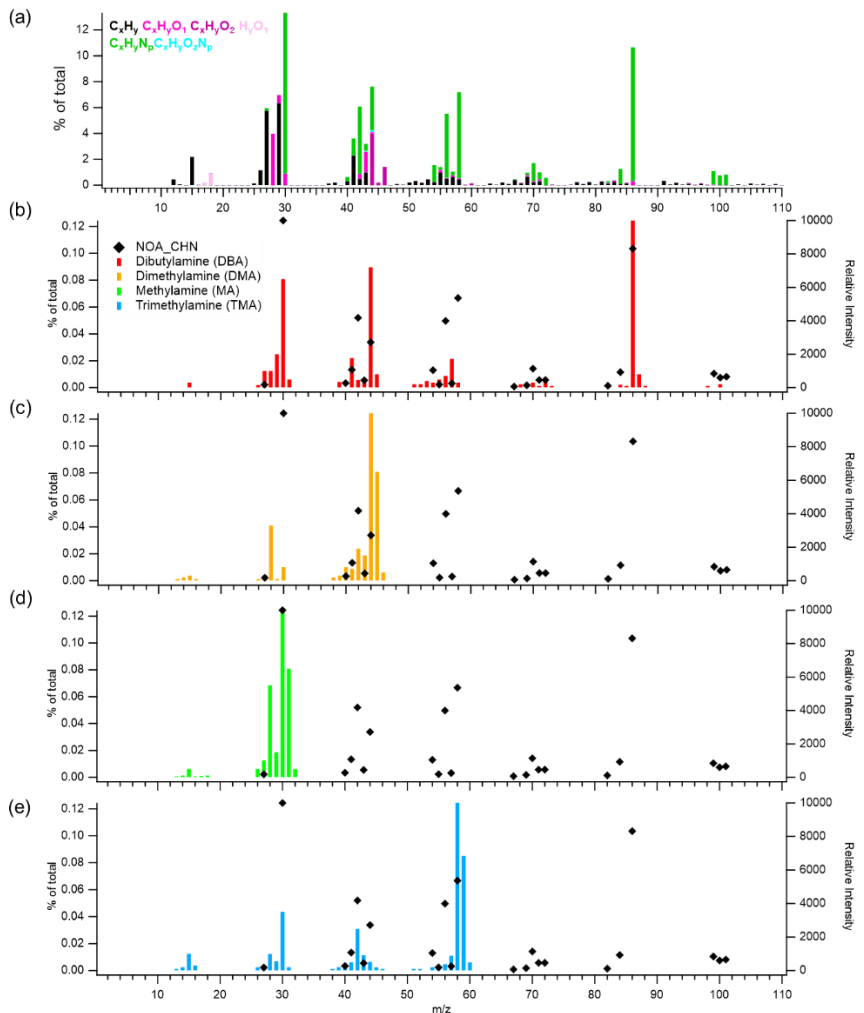
514
515 **Figure 3.** Mass spectra of (a) the NOA factor resolved by PMF analysis in this study, and reference spectra of amines from

516 the NIST library: (b) dibutylamine (DBA), (c) dimethylamine (DMA), (d) methylamine (MA), and (e) trimethylamine

517 (TMA). In panels (b)–(e), the left y-axis indicates the contribution of CHN-containing ions in the NOA factor (% of total),

518 while the right y-axis shows the relative intensity of each compound's mass spectrum from the NIST library.
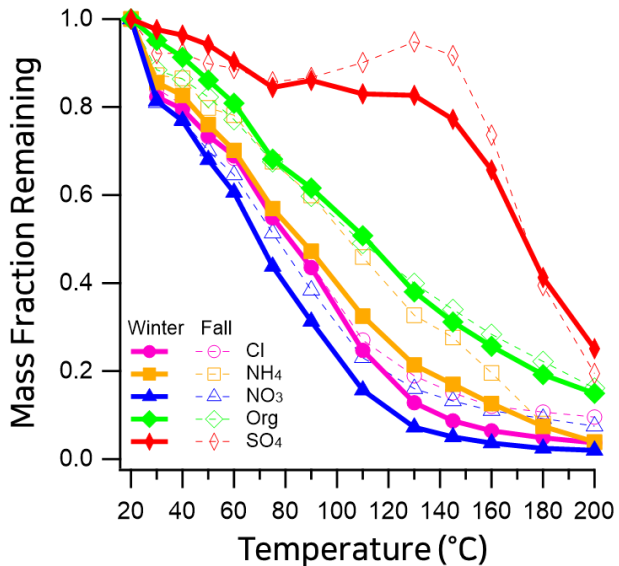
Figure 4. Mass fraction remaining (MFR) of non-refractory (NR) aerosol species measured in Seoul using a thermodenuder coupled to a high-resolution time-of-flight aerosol mass spectrometer (HR-ToF-AMS). Winter 2019 (this study; dashed) is compared with fall 2019 (previously reported; solid) (Jeon et al., 2023). Species include organics (magenta), nitrate (blue), sulfate (orange), ammonium (green), and chloride (red).
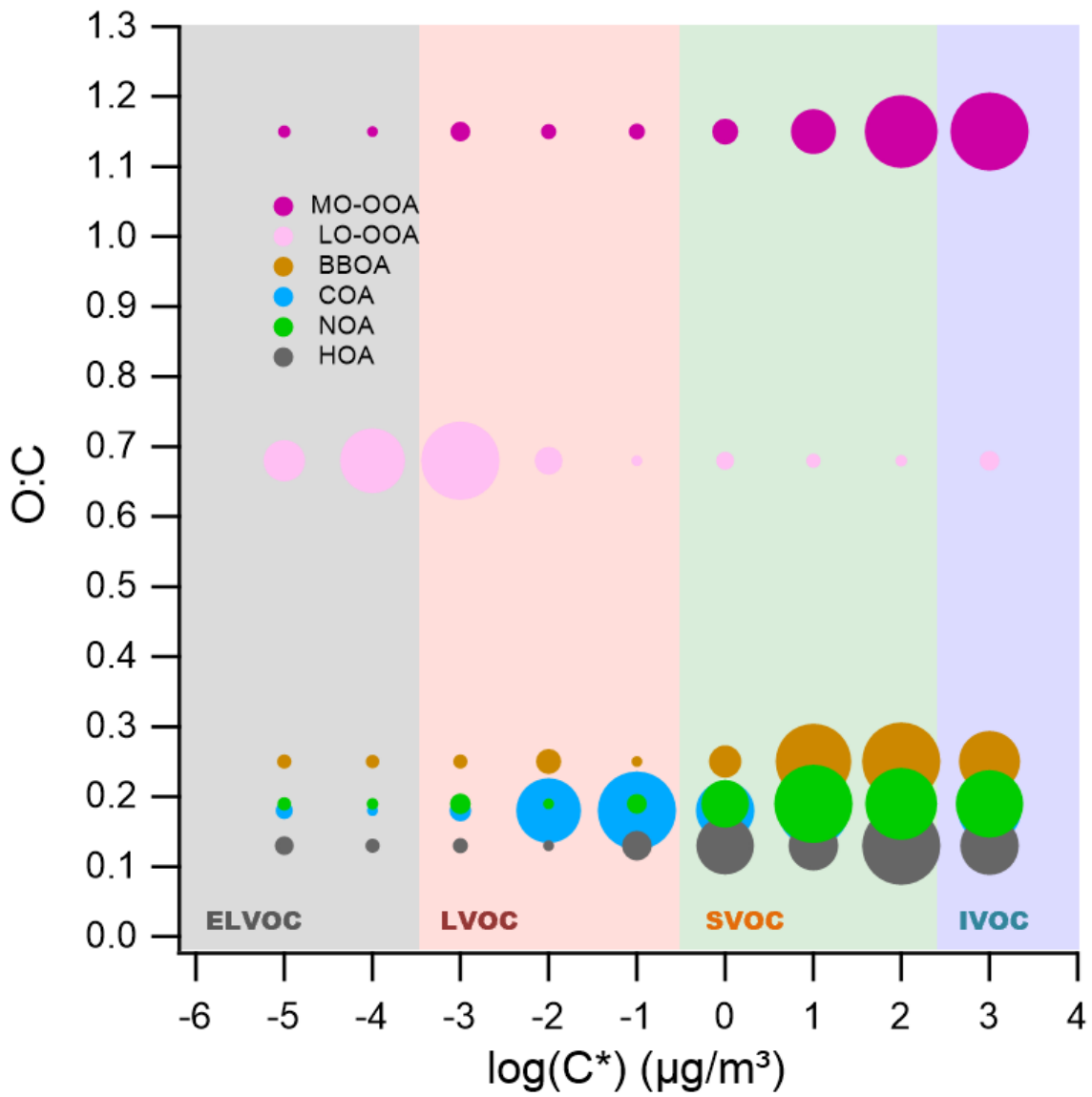
523
Figure 5. Two-dimensional volatility basis set (2D-VBS) representation of organic aerosol (OA) sources identified in winter
2019 in Seoul. The plot illustrates the relationship between the oxygen-to-carbon (O:C) ratio and the effective saturation
concentration (C*) for each OA source resolved via positive matrix factorization (PMF). Solid circles represent the volatility
distribution across C* bins, with marker size proportional to the mass fraction within each bin for the given source. Shaded
regions correspond to different volatility classes: extremely low-volatility organic compounds (ELVOCs), low-volatility
organic compounds (LVOCs), semi-volatile organic compounds (SVOCs), and intermediate-volatility organic compounds
(IVOCs), delineated by their C* values.

23
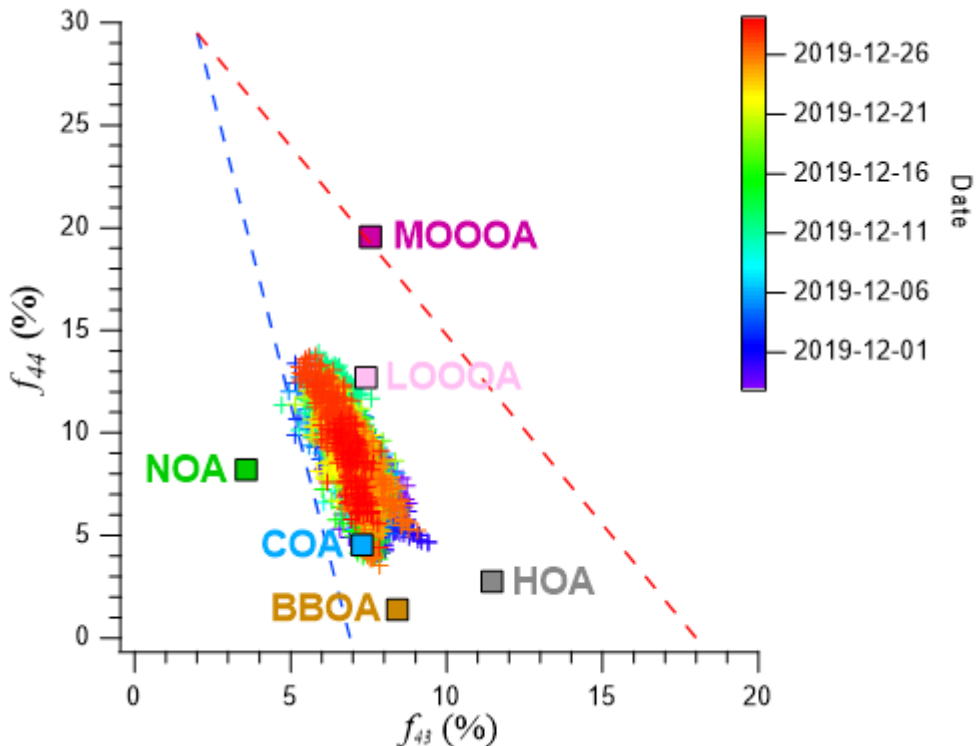
531
Figure 6. scatterplot of f_{44} (CO_2^+) versus f_{43} ($C_2H_3O^+$). for the measured organic aerosol. The data points are color-coded by date to illustrate the temporal variation in OA composition throughout the observation period. The separated OA factors (HOA, COA, BBOA, NOA, LO-OOA, and MO-OOA) are also shown to enable comparison of source contributions and oxidation characteristics. The dashed line represents the typical f_{60} threshold associated with biomass-burning influence, while the triangular boundary indicates the conventional oxidative aging trend in the f_{44}–f_{60} space.

24
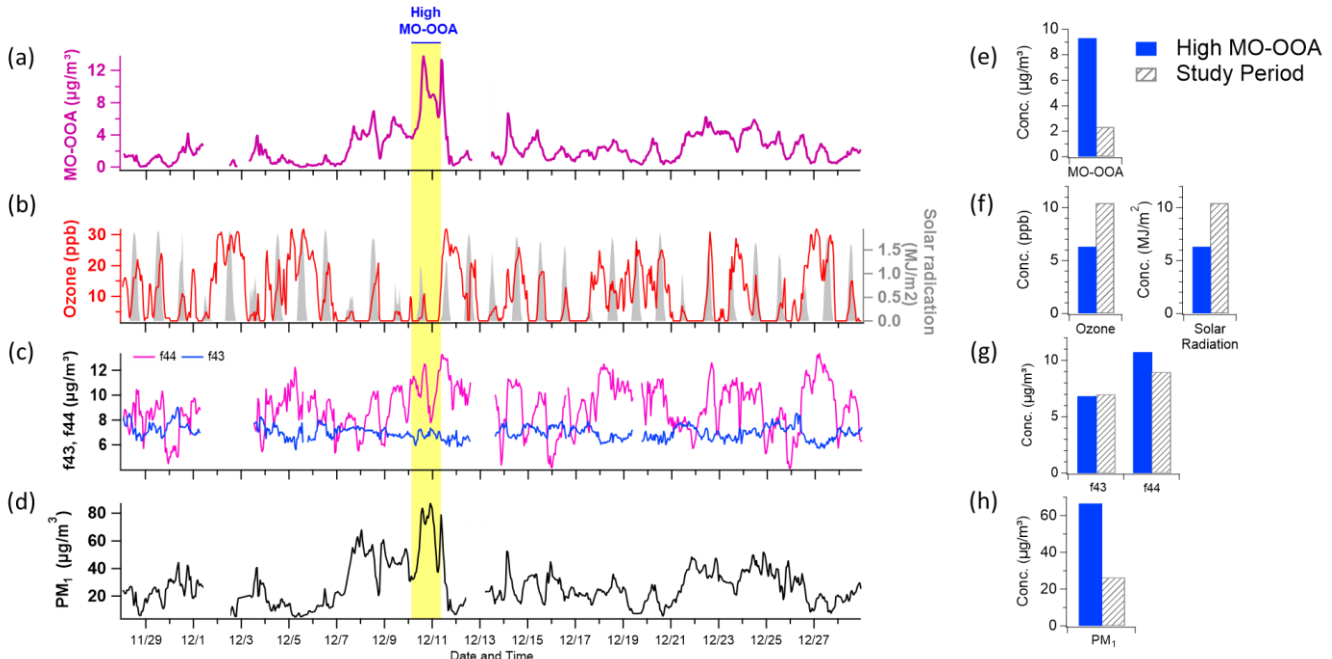
Figure 7. Time series plots of (a) MO-OOA concentration, (b) ozone (O₃) and solar radiation, (c) f_{44} and f_{43} (indicative of oxidation state), and (d) total PM₁ concentration. The period characterized by elevated MO-OOA levels is highlighted in bright yellow. Panels (e)–(f) present comparative distributions of these variables—MO-OOA, O₃ and solar radiation, f_{44} and f_{43}, and PM₁—between the high MO-OOA period (shaded in blue) and the entire measurement period (indicated by gray hatching).

References

Ghim, Y. S., Moon, K.-C., Lee, S., Kim, Y. P., 2005. Visibility trends in Korea during the past two decades. J. Air Waste Manag. Assoc. 55, 73–82. https://doi.org/10.1080/10473289.2005.10464599

Zhao, H., Che, H., Zhang, X., Ma, Y., Wang, Y., Wang, H., Wang, Y., 2013. Characteristics of visibility and particulate matter (PM) in an urban area of Northeast China. Atmos. Pollut. Res. 4, 427–434. https://doi.org/10.5094/APR.2013.049

Hamanaka, R. B., Mutlu, G. M., 2018. Particulate matter air pollution: Effects on the cardiovascular system. Front. Endocrinol. 9, 680. https://doi.org/10.3389/fendo.2018.00680

Manisalidis, I., Stavropoulou, E., Starvropoulos, A., Bezirtzoglou, E., 2020. Environmental and health impacts of air pollution: a review. Front. Public Health 8, 14. https://doi.org/10.3389/fpubh.2020.00014

IPCC, 2021. Climate Change 2021: The Physical Science Basis. Contribution of Working Group I to the Sixth Assessment Report of the Intergovernmental Panel on Climate Change, edited by Masson-Delmotte, V., Zhai, P., Pirani, A., Connors, S.L., Péan, C., Berger, S., et al. Cambridge University Press, Cambridge, UK and New York, NY, USA, pp. 817–922. https://doi.org/10.1017/9781009157896.008

Zhang, Q., Jimenez, J. L., Canagaratna, M. R., Allan, J. D., Coe, H., Ulbrich, I., Alfarra, M. R., Takami, A., Middlebrook, A. M., Sun, Y. L., Dzepina, K., Dunlea, E., Docherty, K., DeCarlo, P., Salcedo, D., Onasch, T. B., Jayne, J. T., Miyoshi, T., Shimono, A., Hatakeyama, N., Takegawa, N., Kondo, Y., Schneider, J., Drewnick, F., Weimer, S., Demerjian, K. L., Williams, P. I., Bower, K. N., Bahreini, R., Cottrell, L., Griffin, R. J., Rautianen, J., Worsnop, D. R., 2007. Ubiquity and dominance of oxygenated species in organic aerosols in anthropogenically-influenced Northern Hemisphere mid-latitudes. Geophys. Res. Lett. 34, L13801. https://doi.org/10.1029/2007GL029979

Jimenez, J. L., Canagaratna, M. R., Donahue, N. M., Prevot, A. S. H., Zhang, Q., Kroll, J. H., ... Worsnop, D. R., 2009. Evolution of organic aerosols in the atmosphere. Science 326, 1525–1529. https://doi.org/10.1126/science.1180353

Hallquist, M., Wenger, J. C., Baltensperger, U., Rudich, Y., Simpson, D., Claeys, M., ... Seinfeld, J. H., 2009. The formation, properties and impact of secondary organic aerosol: current and emerging issues. Atmos. Chem. Phys. 9, 5155–5236. https://doi.org/10.5194/acp-9-5155-2009

Robinson, A. L., Donahue, N. M., Shrivastava, M. K., Weitkamp, E. A., Sage, A. M., Grieshop, A. P., Lane, T. E., Pierce, J. R., Pandis, S. N., 2007. Rethinking organic aerosols: Semivolatile emissions and photochemical aging. Science 315, 1259–1262. https://doi.org/10.1126/science.1133061

Donahue, N. M., Robinson, A. L., Stanier, C. O., Pandis, S. N., 2006. Coupled partitioning, dilution, and chemical aging of semivolatile organics. Environ. Sci. Technol. 40, 2635–2643. https://doi.org/10.1021/es052297c

Ng, N. L., Canagaratna, M. R., Zhang, Q., Jimenez, J. L., Tian, J., Ulbrich, I. M., Kroll, J. H., Docherty, K. S., Chhabra, P. S., Bahreini, R., Murphy, S. M., Seinfeld, J. H., Hildebrandt, L., Donahue, N. M., DeCarlo, P. F., Lanz, V. A., Prévôt, A. S. H., Dinar, E., Rudich, Y., Worsnop, D. R., 2010. Organic aerosol components observed in Northern Hemispheric datasets from Aerosol Mass Spectrometry. Atmos. Chem. Phys. 10, 4625–4641. https://doi.org/10.5194/acp-10-4625-2010

Cappa, C. D., Jimenez, J. L., 2010. Quantitative estimates of the volatility of ambient organic aerosol. Atmos. Chem. Phys. 10, 5409–5424. https://doi.org/10.5194/acp-10-5409-2010

Sinha, A., George, I., Holder, A., Preston, W., Hays, M., Grieshop, A. P., 2023. Development of volatility distributions for organic matter in biomass burning emissions. Environ. Sci. Adv. 3, 11–23. https://doi.org/10.1039/D2EA00080F

Glasius, M., Goldstein, A. H., 2016. Recent discoveries and future challenges in atmospheric organic chemistry. Environ. Sci. Technol. 50, 2754–2764. https://doi.org/10.1021/acs.est.5b05105

Matsui, H., Koike, M., Takegawa, N., Kondo, Y., Griffin, R. J., Miyazaki, Y., Yokouchi, Y., Ohara, T., 2009. Secondary organic aerosol formation in urban air: Temporal variations and possible contributions from unidentified hydrocarbons. J. Geophys. Res. Atmos. 114, D02209. https://doi.org/10.1029/2008JD010164

Jiang, F., Liu, Q., Huang, X., Wang, T., Zhuang, B., Xie, M., 2012. Regional modelling of secondary organic aerosol over China using WRF/Chem. J. Aerosol Sci. 53, 50–61. https://doi.org/10.1016/j.jaerosci.2011.09.003

Li, J., Zhang, M., Wu, F., Sun, Y., Tang, G., 2017. Assessment of the impacts of aromatic VOC emissions and yields of SOA on SOA concentrations with the air quality model RAMS-CMAQ. Atmos. Environ. 158, 105–115. https://doi.org/10.1016/j.atmosenv.2017.03.035

Zhao, B., Wang, S., Donahue, N. M., Jathar, S. H., Huang, X., Wu, W., ... & Hao, J. (2016). Quantifying the effect of organic aerosol aging and intermediate-volatility emissions on regional-scale aerosol pollution in China. Scientific Reports, 6, 28815. https://doi.org/10.1038/srep28815

Kang, H. G., Kim, Y., Collier, S., Zhang, Q., Kim, H., 2022. Volatility of springtime ambient organic aerosol derived with thermodenuder aerosol mass spectrometry in Seoul, Korea. Environ. Pollut. 310, 119203. https://doi.org/10.1016/j.envpol.2022.119203

Huang, X.-F., He, L.-Y., Hu, M., Canagaratna, M. R., Sun, Y., Zhang, Q., Worsnop, D. R., 2010. Highly time-resolved chemical characterization of atmospheric submicron particles during 2008 Beijing Olympic Games

using an Aerodyne High-Resolution Aerosol Mass Spectrometer. Atmos. Chem. Phys. 10, 8933–8945. https://doi.org/10.5194/acp-10-8933-2010

Mohr, C., DeCarlo, P. F., Heringa, M. F., Chirico, R., Slowik, J. G., Richter, R., Reche, C., Alastuey, A., Querol, X., Seco, R., Peñuelas, J., Jiménez, J. L., Crippa, M., Zimmermann, R., Baltensperger, U., Prévôt, A. S. H., 2012. Identification and quantification of organic aerosol from cooking and other sources in Barcelona using aerosol mass spectrometer data. Atmos. Chem. Phys. 12, 1649–1665. https://doi.org/10.5194/acp-12-1649-2012

Xu, L., Kollman, M. S., Song, C., Shilling, J. E., Ng, N. L., 2014. Effects of NOx on the volatility of secondary organic aerosol from isoprene photooxidation. Environ. Sci. Technol. 48, 2253–2262. https://doi.org/10.1021/es404842g

Grieshop, A. P., Logue, J. M., Donahue, N. M., Robinson, A. L., 2009. Laboratory investigation of photochemical oxidation of organic aerosol from wood fires 1: Measurement and simulation of organic aerosol evolution. Atmos. Chem. Phys. 9, 1263–1277. https://doi.org/10.5194/acp-9-1263-2009

Kim, H., Zhang, Q., Bae, G.-N., Kim, J.Y., Lee, S.B., 2017. Sources and atmospheric processing of winter aerosols in Seoul, Korea: Insights from real-time measurements using a high-resolution aerosol mass spectrometer. Atmos. Chem. Phys. 17, 2009–2033. https://doi.org/10.5194/acp-17-2009-2017

DeCarlo, P. F., Kimmel, J. R., Trimborn, A., Northway, M. J., Jayne, A. E., Aiken, A. C., ... & Jimenez, J. L. (2006). Field-deployable, high-resolution, time-of-flight aerosol mass spectrometer. Analytical Chemistry, 78(24), 8281–8289. https://doi.org/10.1021/ac061249

Canagaratna, M. R., Jimenez, J. L., Kroll, J. H., Chen, Q., Kessler, S. H., Massoli, P., ... & Worsnop, D. R. (2015). Elemental ratio measurements of organic compounds using aerosol mass spectrometry: Improved sensitivity and intercomparability. Atmospheric Chemistry and Physics, 15(1), 253–272. https://doi.org/10.5194/acp-15-253-2015

Paatero, P., Tapper, U., 1994. Positive matrix factorization – A nonnegative factor model with optimal utilization of error estimates of data values. Environmetrics 5, 111–126. https://doi.org/10.1002/env.3170050203

Ulbrich, I. M., Canagaratna, M. R., Zhang, Q., Worsnop, D. R., Jimenez, J. L., 2009. Interpretation of organic components from Positive Matrix Factorization of aerosol mass spectrometric data. Atmos. Chem. Phys. 9, 2891–2918. https://doi.org/10.5194/acp-9-2891-2009

Zhang, Q., Jimenez, J. L., Canagaratna, M. R., Ulbrich, I. M., Ng, N. L., Worsnop, D. R., Sun, Y., 2011. Understanding atmospheric organic aerosols via factor analysis of aerosol mass spectrometry: A review. Anal. Bioanal. Chem. 401, 3045–3067. https://doi.org/10.1007/s00216-011-5355-y

Huffman, J. A., Docherty, K. S., Aiken, A. C., Cubison, M. J., Ulbrich, I. M., DeCarlo, P. F., Jimenez, J. L., 2009. Chemically-resolved aerosol volatility measurements from two megacity field studies. Atmos. Chem. Phys. 9, 7161–7182. https://doi.org/10.5194/acp-9-7161-2009

Saha, P. K., Khlystov, A., Grieshop, A. P., 2014. Determining aerosol volatility parameters using a "dual thermodenuder" system: Application to laboratory-generated organic aerosols. Aerosol Sci. Technol. 49, 620–632. https://doi.org/10.1080/02786826.2015.1056769

Zhou, S., Collier, S., Jaffe, D. A., Briggs, N. L., Hee, J., Sedlacek III, A. J., Kleinman, L., & Lewis, K., 2017. Regional influence of wildfires on aerosol chemistry in the western US and insights into atmospheric aging of biomass burning organic aerosol. Atmospheric Chemistry and Physics, 17, 2477–2493. https://doi.org/10.5194/acp-17-2477-2017

Riipinen, I., Pierce, J. R., Donahue, N. M., Pandis, S. N., 2010. Equilibration time scales of organic aerosol inside thermodenuders: Kinetics versus equilibrium thermodynamics. Atmos. Environ. 44, 597–607. https://doi.org/10.1016/j.atmosenv.2009.11.022

Karnezi, E., Riipinen, I., Pandis, S. N., 2014. Measuring the atmospheric organic aerosol volatility distribution: a theoretical analysis. Atmos. Meas. Tech. 7, 2953–2965. https://doi.org/10.5194/amt-7-2953-2014

Chen, Y., Wang, Z., Wang, Y., Zheng, X., Fu, P., Kawamura, K., Zhang, Y., 2021. Characterization of nitrogen-containing organic aerosol in Guangzhou, China: seasonal variation, formation mechanism and source apportionment. Atmos. Chem. Phys. 21, 4329–4344. https://doi.org/10.5194/acp-21-4329-2021

Hayes, P. L., Ortega, A. M., Cubison, M. J., Froyd, K. D., Zhao, Y., Cliff, S. S., ... Jimenez, J. L., 2013. Organic aerosol composition and sources in Pasadena, California, during the 2010 CalNex campaign. J. Geophys. Res. Atmos. 118, 9233–9257. https://doi.org/10.1002/jgrd.50530

Sun, Y., Jiang, Q., Wang, Z., Fu, P., Li, J., Yang, T., Yin, Y., 2011. Investigation of the sources and evolution processes of severe haze pollution in Beijing in January 2013. J. Geophys. Res. Atmos. 119, 4380–4398. https://doi.org/10.1002/2014JD021641

Baek, K. M., Park, E. H., Kang, H., Ji, M. J., Park, H. M., Heo, J & Kim, H., 2022. Seasonal characteristics of atmospheric water-soluble organic nitrogen in PM2.5 in Seoul, Korea: Source and atmospheric processes of free amino acids and aliphatic amines. Science of the Total Environment, 807, 150785. https://doi.org/10.1016/j.scitotenv.2021.152335

Rovelli, G., Miles, R. E. H., Reid, J. P., and Clegg, S. L.: Hygroscopic properties of aminium sulfate aerosols, Atmos. Chem. Phys., 17, 4369–4385, https://doi.org/10.5194/acp-17-4369-2017, 2017.

Ge, X., Wexler, A. S., Clegg, S. L., 2011. Atmospheric amines – Part I. A review. Atmos. Environ. 45, 524–546. https://doi.org/10.1016/j.atmosenv.2010.10.012

He, L.-Y., Lin, Y., Huang, X. F., Guo, W. W., Niu, J. L., Shen, Y. F., Sen, J., and Hu, M.: Characterization of high-resolution aerosol mass spectra of primary organic aerosol emissions from Chinese cooking and biomass burning, *Atmos. Chem. Phys.*, 10, 11535–11543, https://doi.org/10.5194/acp-10-11535-2010, 2010

You, Y., Renbaum-Wolff, L., Carreras-Sospedra, M., Dabdub, D., Bertram, A. K., Martin, S. T., et al., 2014. Images reveal that amines promote the heterogeneous reaction of epoxides in model organic aerosols. J. Phys. Chem. Lett. 5, 3211–3215. https://doi.org/10.1021/jz501268k

Yao, L., Wang, M. Y., Wang, X. K., Zhang, W. Q., Liu, Y., Li, L., et al., 2016. Atmospheric new particle formation from sulfuric acid and amines in a Chinese megacity. Sci. Bull. 61, 939–945. https://doi.org/10.1007/s11434-016-1083-0

Kim, H., Zhang, Q., Sun, Y., Bae, G. N., Lee, B. E., Park, K., ... & Kim, Y. J. 2020. Measurement report: Characterization of severe spring haze episodes and influences of long-range transport in the Seoul metropolitan area in March 2019. Atmospheric Chemistry and Physics, 20(18), 11527–11545. https://doi.org/10.5194/acp-20-11527-2020

Jeon, J., Chen, Y., Kim, H., 2023. Influence of meteorology on emission sources and physicochemical properties of particulate matter in Seoul, Korea during heating period. Atmos. Environ. 301, 119733. https://doi.org/10.1016/j.atmosenv.2023.119733

Zhang, Q., Alfarra, M. R., Worsnop, D. R., Allan, J. D., Coe, H., Canagaratna, M. R., ... & Jimenez, J. L. 2005. Deconvolution and quantification of hydrocarbon-like and oxygenated organic aerosols based on aerosol mass spectrometry. Environmental Science & Technology, 39(13), 4938–4952. https://doi.org/10.1021/es048568l

Simoneit, B. R. T. 2002. Biomass burning – a review of organic tracers for smoke from incomplete combustion. Applied Geochemistry, 17(3), 129–162. https://doi.org/10.1016/S0883-2927(01)00061-0

Cubison, M. J., Ortega, A. M., Hayes, P. L., Farmer, D. K., Day, D., Lechner, M. J., ... & Jimenez, J. L. 2011. Effects of aging on organic aerosol from open biomass burning smoke in aircraft and laboratory studies. Atmospheric Chemistry and Physics, 11(23), 12049–12064. https://doi.org/10.5194/acp-11-12049-2011

Xu, L., Williams, L. R., Young, D. E., Allan, J. D., Coe, H., Massoli, P., Fortner, E., Chhabra, P., Herndon, S., Brooks, W. A., Jayne, J. T., Worsnop, D. R., Aiken, A. C., Liu, S., Gorkowski, K., Dubey, M. K., Fleming, Z. L., Visser, S., Prévôt, A. S. H., Ng, N. L., 2016. Wintertime aerosol chemical composition, volatility, and spatial variability in the Greater London Area. Atmos. Chem. Phys. 16, 1139–1160. https://doi.org/10.5194/acp-16-1139-2016

Feng, T., Wang, Y., Hu, W., Zhu, M., Song, W., Chen, W., ... Wang, X., 2023. Impact of aging on the sources, volatility, and viscosity of organic aerosols in Chinese outflows. Atmos. Chem. Phys. 23, 611–636. https://doi.org/10.5194/acp-23-611-2023

Scott, W. D., & Cattell, F. C. R. 1979. Vapor pressure of ammonium sulfates. Atmospheric Environment (1967), 13(6), 987–1000. https://doi.org/10.1016/0004-6981(79)90174-4

Donahue, N. M., Robinson, A. L., Pandis, S. N., 2009. Atmospheric organic particulate matter: From smoke to secondary organic aerosol. Atmos. Environ. 43, 94–106. https://doi.org/10.1016/j.atmosenv.2008.09.055

Ehn, M., Thornton, J. A., Kleist, E., Sipilä, M., Junninen, H., Pullinen, I., ... & Kulmala, M. 2014. A large source of low-volatility secondary organic aerosol. Nature, 506(7489), 476–479. https://doi.org/10.1038/nature13032

Kroll, J. H., Smith, J. D., Che, D. L., Kessler, S. H., Worsnop, D. R., Wilson, K. R., 2009. Measurement of fragmentation and functionalization pathways in the heterogeneous oxidation of oxidation organic aerosol. Environ. Sci. Technol. 43, 7826–7833. https://doi.org/10.1021/es901683r

Xu, W., Takeuchi, M., Chen, C., Qiu, Y., Xie, C., Xu, W., Ma, N., Worsnop, D. R., Ng, N. L., and Sun, Y.: Estimation of particulate organic nitrates from thermodenuder–aerosol mass spectrometer measurements in the North China Plain, 14, 3693–3705, https://doi.org/10.5194/amt-14-3693-2021, 2021.

Cao, L.-M., Huang, X.-F., Li, Y.-Y., Hu, M., He, L.-Y., 2018. Volatility measurement of atmospheric submicron aerosols in an urban atmosphere in southern China. Atmos. Chem. Phys. 18, 1729–1743. https://doi.org/10.5194/acp-18-1729-2018

Xu, W., Xie, C., Karnezi, E., Zhang, Q., Wang, J., Pandis, S.N., Ge, X., Zhang, J., An, J., Wang, Q., et al., 2019. Summertime aerosol volatility measurements in Beijing, China. Atmos. Chem. Phys. 19, 10205–10216. https://doi.org/10.5194/acp-19-10205-2019

Allan, J. D., Alfarra, M. R., Bower, K. N., Williams, P. I., Gallagher, M. W., Jimenez, J. L., McDonald, A. G., Nemitz, E., Canagaratna, M. R., and Coe, H.: Quantitative sampling using an Aerodyne aerosol mass spectrometer—2. Measurements of fine particulate chemical composition in two U.K. cities, J. Geophys. Res.-Atmos., 108, 4091, 2003, https://doi.org/10.1029/2002JD002359.

Berndt, T., Richters, S., Jokinen, T., et al.: Hydroxyl radical-induced formation of highly oxidized organic compounds, Nat. Commun., 7, 13677, 2016, https://doi.org/10.1038/ncomms13677.

Bianchi, F., Kurtén, T., Riva, M., et al.: Highly oxygenated organic molecules (HOM) from gas-phase autoxidation involving peroxy radicals: A key contributor to atmospheric aerosol, Chem. Rev., 119, 3472–3509, 2019, https://doi.org/10.1021/acs.chemrev.8b00395.

Brown, S. S. and Stutz, J.: Nighttime radical observations and chemistry, Chem. Soc. Rev., 41, 6405–6447, 2012, https://doi.org/10.1039/C2CS35181A.

Canagaratna, M. R., Jayne, J. T., Jimenez, J. L., et al.: Chemical and microphysical characterization of ambient aerosols with the Aerodyne aerosol mass spectrometer, Mass Spectrom. Rev., 26, 185–222, 2007, https://doi.org/10.1002/mas.20115.

Chhabra, P. S., Ng, N. L., Canagaratna, M. R., et al.: Elemental composition and oxidation of chamber organic aerosol, Atmos. Chem. Phys., 11, 8827–8841, 2011, https://doi.org/10.5194/acp-11-8827-2011.

D'Ambro, E. L., Schobesberger, S., Gaston, C. J., et al.: Molecular composition and volatility of isoprene photochemical oxidation secondary organic aerosol under low- and high-NOx conditions, Atmos. Chem. Phys., 17, 159–174, 2017, https://doi.org/10.5194/acp-17-159-2017.

Donahue, N. M., Epstein, S. A., Pandis, S. N., and Robinson, A. L.: A two-dimensional volatility basis set – Part 1: Organic-aerosol mixing thermodynamics, Atmos. Chem. Phys., 11, 3303–3318, 2011, https://doi.org/10.5194/acp-11-3303-2011.

Faulhaber, A. E., Thomas, B. M., Jimenez, J. L., et al.: Characterization of a thermodenuder–particle beam mass spectrometer system for the study of organic aerosol volatility and composition, Atmos. Meas. Tech., 2, 15–31, 2009, https://doi.org/10.5194/amt-2-15-2009.

Ge, X., Wexler, A. S., and Clegg, S. L.: Atmospheric amines – Part III: Photochemistry and toxicity, Atmos. Environ., 45, 561–591, 2011, https://doi.org/10.1016/j.atmosenv.2010.11.050.

Gil, J., Lee, Y., and Kim, Y. P.: Characteristics of HONO and its impact on O3 formation in the Seoul Metropolitan Area during KORUS-AQ, Atmos. Environ., 246, 118032, 2021, https://doi.org/10.1016/j.atmosenv.2020.118032.

Han, K.-M., Kim, D.-G., Kim, J., et al.: Crop residue burning emissions and impact on particulate matter over South Korea, Atmosphere, 13, 559, 2022, https://doi.org/10.3390/atmos13040559.

Hanson, D. R., McMurry, P. H., Jiang, J., et al.: Ambient pressure proton transfer mass spectrometry: detection of amines and ammonia, Environ. Sci. Technol., 45, 8881–8888, 2011, https://doi.org/10.1021/es2018817.

Hennigan, C. J., Sullivan, A. P., Collett, J. L., Jr., and Robinson, A. L.: Levoglucosan stability in biomass burning particles exposed to hydroxyl radicals, Geophys. Res. Lett., 37, L09806, 2010, https://doi.org/10.1029/2010GL043088.

Huffman, J. A., Ziemann, P. J., Jayne, J. T., et al.: Development and characterization of a fast-stepping thermodenuder for chemically resolved aerosol volatility measurements, Aerosol Sci. Technol., 42, 395–407, 2008, https://doi.org/10.1080/02786820802104981.

Kim, K., Park, R., Lee, Y., et al.: An investigation into atmospheric nitrous acid (HONO) and its sources in East Asia, Atmos. Chem. Phys., 24, 12575–12593, 2024, https://doi.org/10.5194/acp-24-12575-2024.

Kroll, J. H. and Seinfeld, J. H.: Chemistry of secondary organic aerosol: Formation and evolution of low-volatility organics in the atmosphere, Atmos. Environ., 42, 3593–3624, 2008, https://doi.org/10.1016/j.atmosenv.2008.01.003.

Kroll, J., Donahue, N., Jimenez, J., et al.: Carbon oxidation state as a metric for describing the chemistry of atmospheric organic aerosol, Nat. Chem., 3, 133–139, 2011, https://doi.org/10.1038/nchem.948.

Kwon, S., Won, S. R., Lim, H. B., et al.: Relationship between PM1.0 and PM2.5 in urban and background areas of the Republic of Korea, Atmos. Pollut. Res., 14, 101858, 2023, https://doi.org/10.1016/j.apr.2023.101858.

Lamb, K. D., Kim, B.-G., and Kim, S.-W.: Estimating source-region influences on black carbon in South Korea using the BC/CO ratio, J. Geophys. Res.-Atmos., 123, 11, 2018, https://doi.org/10.1029/2018JD029257.

Lambe, A. T., Onasch, T. B., Massoli, P., et al.: Transitions from Functionalization to Fragmentation Reactions of Laboratory Secondary Organic Aerosol (SOA) Generated from the OH Oxidation of Alkane Precursors, Environ. Sci. Technol., 46, 5430–5437, 2012, https://doi.org/10.1021/es300274t.

López-Hilfiker, F. D., Mohr, C., Ehn, M., et al.: A novel method for online analysis of gas and particle composition: description and evaluation of a Filter Inlet for Gases and AEROsols (FIGAERO), Atmos. Meas. Tech., 7, 983–1001, 2014, https://doi.org/10.5194/amt-7-983-2014.

López-Hilfiker, F. D., Mohr, C., Ehn, M., et al.: Molecular composition and volatility of organic aerosol in the Southeastern U.S. using FIGAERO–CIMS with comparison to AMS, Environ. Sci. Technol., 50, 2200–2209, 2016, https://doi.org/10.1021/acs.est.5b04769.

Mao, J., Wang, L., Lu, C., et al.: High-resolution modeling of gaseous methylamines over a polluted region in China: source-dependent emissions and implications of spatial variations, Atmos. Chem. Phys., 18, 7933–7950, 2018, https://doi.org/10.5194/acp-18-7933-2018.

Matsui, H., Koike, M., Kondo, Y., et al.: An estimation of the organic aerosol component in PM2.5 using AMS and CMB models, J. Geophys. Res.-Atmos., 114, D21203, 2009, https://doi.org/10.1029/2009JD012170.

Nault, B. A., Campuzano-Jost, P., Day, D. A., et al.: Secondary organic aerosol production from local emissions dominates over Seoul during KORUS-AQ, Atmos. Chem. Phys., 18, 17769–17800, 2018, https://doi.org/10.5194/acp-18-17769-2018.

Nielsen, C. J., Herrmann, H., and Weller, C.: Atmospheric chemistry and environmental impact of the use of amines in carbon capture and storage (CCS), Chem. Soc. Rev., 41, 6684–6704, 2012, https://doi.org/10.1039/C2CS35059A.

Slater, E. J., Gkatzoflias, D., Wang, Y., et al.: Elevated levels of OH observed in haze events during wintertime Beijing, Atmos. Chem. Phys., 20, 14847–14871, 2020, https://doi.org/10.5194/acp-20-14847-2020.

Sun, Y., Zhang, Q., Schwab, J. J., et al.: Characterization of the sources and properties of organic aerosol from AMS measurements during a winter campaign in Beijing, China, Atmos. Chem. Phys., 10, 8951–8971, 2010, https://doi.org/10.5194/acp-10-8951-2010.

Tiszenkel, L., Flynn, J. H., and Lee, S.-H.: Measurement report: Urban ammonia and amines in Houston, Texas, Atmos. Chem. Phys., 24, 11351–11363, 2024, https://doi.org/10.5194/acp-24-11351-2024.

Yoo, H., Lee, H., and Kim, Y. P.: Insights from single-particle analysis: submicron aerosol composition in Seoul during KORUS-AQ, Atmos. Chem. Phys., 24, 853–872, 2024, https://doi.org/10.5194/acp-24-853-2024.

Ziemann, P. J. and Atkinson, R.: Kinetics, products, and mechanisms of secondary organic aerosol formation from gas-phase reactions of organic compounds, Chem. Soc. Rev., 41, 6582–6605, 2012, https://doi.org/10.1039/C2CS35122F.

Paciga, A., Young, D. E., Ward, M. W., et al.: Volatility of organic aerosol and its components in the megacity of Paris, Atmos. Chem. Phys., 16, 2013–2031, 2016, https://doi.org/10.5194/acp-16-2013-2016.

Ge, X., Wexler, A. S., and Clegg, S. L.: Atmospheric amines – Part II. Thermodynamic properties and gas-particle partitioning, Atmos. Chem. Phys., 11, 55–69, 2011, https://doi.org/10.5194/acp-11-55-2011.

Xu, W., Sun, Y., Wang, Q., et al.: Seasonal characterization of organic nitrogen in atmospheric aerosols using high-resolution aerosol mass spectrometry in Beijing, China, ACS Earth Space Chem., 1, 649–658, 2017, https://doi.org/10.1021/acsearthspacechem.7b00106.

Sun, Y. L., Zhang, Q., Schwab, J. J., et al.: Characterization of the sources and processes of organic and inorganic aerosols in New York City with a high-resolution time-of-flight aerosol mass spectrometer, Atmos. Chem. Phys., 11, 1581–1602, 2011, https://doi.org/10.5194/acp-11-1581-2011.

Saarikoski, S., Carbone, S., Decesari, S., et al.: Chemical characterization of springtime submicrometer aerosol in Po Valley, Italy, Atmos. Chem. Phys., 12, 8401–8421, 2012, https://doi.org/10.5194/acp-12-8401-2012.

Silva, P. J., Erupe, M. E., Price, D., et al.: Trimethylamine as precursor to secondary organic aerosol formation via nitrate radical reaction in the atmosphere, Environ. Sci. Technol., 42, 4689–4696, 2008, https://doi.org/10.1021/es703016v

EPA: EPA Positive Matrix Factorization (PMF) 5.0 Fundamentals and User Guide, U.S. Environmental Protection Agency, 2014. https://www.epa.gov/sites/default/files/2015-02/documents/pmf_5.0_user_guide.pdf

Waked, A., Favez, O., Alleman, L.Y., Piot, C., Petit, J.E., Delaunay, T., Verlinden, E., Jayne, J., Sciare, J., 2014. Source apportionment of PM10 in a north-western Europe regional urban background site (Lens, France) using

positive matrix factorization and including primary emissions. Atmos. Chem. Phys. 14, 3325–3346. https://doi.org/10.5194/acp-14-3325-2014

Soleimani, M., Ebrahimi, Z., Mirghaffari, N., Naseri, M., 2022. Source identification of polycyclic aromatic hydrocarbons associated with fine particulate matters (PM2.5) in Isfahan City, Iran, using diagnostic ratio and PMF model. Environ. Sci. Pollut. Res. 29, 30310–30326. https://doi.org/10.1007/s11356-021-17635-8

Allan, J. D., Williams, P. I., Morgan, W. T., et al.: Contributions from transport, solid fuel burning and cooking to primary organic aerosols in two UK cities, Atmos. Chem. Phys., 10, 647–668, 2010, https://doi.org/10.5194/acp-10-647-2010.

Mohr, C., DeCarlo, P. F., Heringa, M. F., et al.: Identification and quantification of organic aerosol from cooking and other sources in Barcelona using aerosol mass spectrometer data, Atmos. Chem. Phys., 12, 1649–1665, 2012, https://doi.org/10.5194/acp-12-1649-2012.

Sun, Y.-L., Zhang, Q., Schwab, J. J., et al.: Characterization of the sources and processes of organic aerosols in New York City with a high-resolution time-of-flight aerosol mass spectrometer, Atmos. Chem. Phys., 11, 1581–1602, 2011, https://doi.org/10.5194/acp-11-1581-2011.